Polymer 50 (2009) 5298–5307

Contents lists available at ScienceDirect

Polymer

journal homepage: www.elsevier.com/locate/polymer

Relationship between free volume properties and structure of poly(3-hydroxybutyrate-co-3-hydroxyvalerate) membranes via various crystallization conditions

Mei-Ling Cheng [a], Yi-Ming Sun [a,b,*]

[a] Department of Chemical Engineering and Materials Science, Yuan Ze University, Chung-Li, Taoyuan 32003, Taiwan
[b] R&D Center for Membrane Technology, Chung Yuan University, Chung-Li, Taoyuan 32023, Taiwan

ARTICLE INFO

Article history:
Received 15 April 2009
Received in revised form
27 August 2009
Accepted 12 September 2009
Available online 16 September 2009

Keywords:
Free volume
Crystallization temperature
Lamellar structure

ABSTRACT

The relationship between the crystalline structure and the free volume properties within the amorphous phase of poly(3-hydroxybutyrate-co-3-hydroxyvalerate) (PHBV) membranes, which were prepared via isothermal crystallization processes at various crystallization temperatures, was investigated. From the data of positron annihilation lifetime (PAL) spectroscopy over a temperature range of 25–90 °C, the temperature dependence of free volume size, amount, distribution, and relative fractional free volume and thermal expansion behaviors of free volume were discussed. The existence of a rigid-amorphous fraction (RAF) which constrained long-range motions in the semi-crystalline polymer was demonstrated by DSC trace and considered to interpret the temperature dependence of those free volume properties. Based on the crystallization conditions, the effect of the crystallization rate of PHBV polymer was proposed to explain the thermal expansion coefficients of free volume size. The membranes crystallized at faster crystallization rate would accompany higher thermal expansion coefficients of free volume size and the larger free volume size at higher temperatures. Larger distribution of the free volume size and higher thermal expansivity of *o*-Ps lifetime dispersion ($d\sigma/dt$) of isothermally melt-crystallized membranes were observed as a result of the bimodal distribution of the lamellar periodicity, which was obtained by small-angle X-ray scattering (SAXS), and less amount of RAF than that of a cold-crystallized membrane. Conclusively, free volume size and thermal expansion of the free volume in PHBV membranes were affected by the kinetics of crystallization; comparatively, the total amount of free volume and fractional free volume were determined by the final crystallinity. The size distribution of free volume was associated with the crystalline lamellar structure which was dominated by the crystallization conditions.

1. Introduction

A polymer is composed of entangled polymer chains and the space between polymer chains is generally called free volume, which means free moving open space. Free volume concept in polymers is based on the model that molecules or chain segments can rearrange themselves freely therefore dynamical open space may be created during the process. The holes of free volume are not fixed in designated positions but in fact flowing around inside the polymer matrix due to the segmental rearrangement. The so-called fractional free volume (FFV), therefore, is an averaged fraction of the open space within the polymer at all times. Since very early years, it has been widely utilized to describe properties of polymers, such as the mechanical viscoelasticity [1], viscosity [2], glass transition [3], relaxation [4], physical aging [5], and transport properties [6].

In semi-crystalline polymers, the free volume properties appear to be much more complicated than that in an amorphous polymer due to the complex morphology which includes crystalline and amorphous regions. When polymers are crystallized from the bulk, the classical crystallization process in which spherulitic structure grows during primary crystallization is followed [7]. The structure of spherulites is generally modeled as stacks of individual lamellar crystalline plates. This microstructure consists of a distribution of lamellar stacks with relatively large interlamellar amorphous regions in which long-range motions are restricted. This has been

* Corresponding author. Department of Chemical Engineering and Materials Science, Yuan Ze University, Chung-Li, Taoyuan 32003, Taiwan. Tel.: +886 3 4638800x2558; fax: +886 3 4559373.
E-mail address: cesunym@saturn.yzu.edu.tw (Y.-M. Sun).

0032-3861/$ – see front matter © 2009 Elsevier Ltd. All rights reserved.
doi:10.1016/j.polymer.2009.09.035

associated with the existence of a rigid-amorphous fraction (RAF), which corresponds to the less movable fraction of the amorphous material despite lacking of large range order [8]. The RAF was treated as an excess immobile fraction in addition to that included in the crystals and was observed by the dynamics of the α-relaxation measured by dielectric spectroscopy [9]. On the side, the non-crystalline amorphous region between lamellar stacks is liquid-like amorphous and expected to exhibit properties, such as T_g, as the completely amorphous bulk polymers. It may be termed as mobile amorphous fraction (MAF). The concept of RAF in addition to crystalline phase and MAF has been investigated to explain properties of semi-crystalline polymers in recent years [10–13]. Moreover, the degree of crystallinity in a polymer depends to a large degree on the chemical structure as well as the crystallization procedure that the polymer has experienced. It is possible to alter the crystallinity and the crystalline structure by varying the kinetics with which the crystallization takes place. The kinetics of crystallization included the nucleation rate (N), the crystal growth rate (G), and the overall crystallization rate (K) [14]. The overall crystallization rate is a function of the crystallinity ($X(t)$), the crystallization time (t), and the crystallization rate constant (k), which is affected by the nucleation and crystal growth rates directly ($k = k(N, G)$), at a constant temperature. Generally, the overall crystallization rate is controlled by the thermodynamic driving force and the chain mobility, therefore, a maximum of crystallization rate is observed. Above the crystallization temperature at maximum rate ($T_{c,max}$), the crystallization rate decreases with increasing temperature due to decreased nucleation rate (thermodynamically controlled behavior). Below the $T_{c,max}$, the crystallization rate decreases with decreasing temperature due to decreased molecular motion as the glass transition is approached (mobility controlled behavior). Accordingly, the morphology and structure of crystalline phase should be considered as an important factor affecting the free volume size and the size distribution in the amorphous region.

A positron annihilation lifetime (PAL) spectroscopy method has been developed to be an important tool for studying the free volume properties of polymers over the past two decades [15–18]. When a positron injects into a material media, it annihilates with emission of gamma radiation. Because of the interaction between the positron and electrons in the media, positron may form a bound state with an electron before annihilation, which yields a positronium, Ps. Depending on the spin states of the two particles, Ps may form into different states: *para*-positronium (*p*-Ps, singlet state) for anti-parallel spins and *ortho*-positronium (*o*-Ps, triplet state) for parallel spins. The intrinsic vacuum lifetimes are 0.125 ns (τ_1) and 142 ns (τ_3) for *p*-Ps and *o*-Ps, respectively. Free positrons annihilate with lifetime in the rage of 0.3–0.4 ns (τ_2). However, the observed *o*-Ps lifetime in molecular substrates decreases typically to a few nanosecond ranges due to collisions of Ps with molecules (pick-off annihilation) [19]. If *o*-Ps localized in a free volume hole in the amorphous polymer, its lifetime is between 2 and 5 ns, and highly sensitive to the size of the free volume. The smaller the hole is, the higher the frequency of collisions and the shorter the *o*-Ps life are.

In the current work, the temperature dependence of positron/Ps annihilation parameters in semi-crystalline poly(3-hydroxybutyrate-co-3-hydroxyvalerate) (PHBV) is studied in the temperature range between 25 and 90 °C. PHBV is a naturally derived biodegradable polymer that has better processing and mechanical properties than poly(3-hydroxybutyrate) (PHB) homopolymer as the 3HV (3-hydroxyvalerate) units in PHBV can reduce the melting temperature and brittleness [20]. PHBV polymer exhibits the phenomenon of isodimorphism, cocrystallization of the two monomer units in either of the homopolymer crystal lattices, as the constituent composition is varied [21]. As a consequence of the cocrystallization of the 3HB (3-hydroxybutyrate) and 3HV units, PHBV polymer shows a substantial crystalline phase over the whole composition range. In addition, a wide range of physical properties of PHBV copolymer are depending on the 3HV composition. A number of reports have exploited that PHBV copolymers offer suitable properties for making coated paper and decorative home goods [22,23].

In previous studies [16,24,25], the relationship between crystallinity and free volume properties of semi-crystalline polymers was reported. They observed that the *o*-Ps annihilation parameter I_3 value, which means the amount of free volume, decreased with an increasing amount of crystallinity. However, the study about the effect of crystalline structure at the nanoscale and/or molecular levels on the free volume characteristics was very few. We have investigated the free volume properties of non-isothermally crystallized PHBV membranes and discussed the influence of the cooling rate on the free volume properties [26]. In this work, PHBV polymer is processed via the isothermal melt-crystallization procedures at different crystallization temperatures to form a series of membranes with different morphology and degree of crystallinity. The objective of this study is to investigate the changes of the polymer free volume properties subjected to the controlled crystallization conditions. We attempt to distinguish the difference of the microstructure of PHBV polymer prepared by different crystallization procedures and to conclude their effect on the free volume characteristics.

2. Experimental

2.1. Material

Poly(3-hydroxybutyrate-co-3-hydroxyvalerate) (PHBV) with a 3-hydroxyvalerate (3HV) comonomer content of 5 mol% was supplied by Aldrich, Inc. (USA). The weight-average molecular weight ($\overline{M}_w$) was about 400,000 g/mol and the polydispersity index (PDI) was about 2 as determined by gel-permeation chromatography (GPC) using polystyrene standards and chloroform as a solvent. The polymer powder showed a glass temperature (T_g) at 0 °C and melting temperature around 162 °C measured by DSC experiment with two heating and one cooling processes which scanned from −40 to 200 °C with a scanning of ±10 °C/min.

2.2. Membrane preparation

The membranes were prepared by a compression-molding method performed with a molding test press (GT-7014, Gotech, Taiwan). The polymer powder was sandwiched between two flat stainless steel plates (220 × 220 mm^2, 0.75 mm of the thickness) and the plate molding assembly was placed in the hot press. The samples were melted at 170 °C (above the melting point of PHBV powders, T_m, 162 °C as measured) for 5 min, and then were compression-molded under a pressure of 9.8 MPa at 170 °C for 15 min. Once melted, the molding assembly was removed from the hot press machine and put into an oven at one of the following predetermined crystallization temperatures: 50, 70, 90, 110, and 130 °C, respectively. Hereafter, Iso50, Iso70, Iso90, Iso110, and Iso130 are used to denote these isothermally crystallized membranes, respectively, in this manuscript. The membranes were placed in the oven for 48 h to complete the isothermal crystallization treatment. After crystallization process, all the membranes were kept in a desiccator, to avoid any water moisture sorption before further characterization, at room temperature. The average thickness of the membranes was around 55 μm measured by a digital micrometer (IDF-112, Mitutoyo, Japan).

In addition, cold-crystallized membranes were prepared via a rapid-cooling process [26]. Following the same melting process

for preparing the isothermally crystallized samples, the melted sample was quenched to 0 °C in an icebox for 10 min and then kept in a desiccator at room temperature. The samples crystallized at room temperature followed the cold-crystallization procedure. Details can be found in our previous report [26].

2.3. Thermal properties and crystallinity

Thermal characterization was carried out with a DSC instrument (DSC7, Perkin–Elmer, USA) equipped with an intra-cooler. The temperature scale was calibrated with indium standard. The melt-molded membranes of around 6–9 mg were hermetically sealed in an aluminum pan for the measurements. Under a nitrogen atmosphere, samples were scanned from −40 °C to 200 °C with a heating rate of 10 °C/min. From the melting endotherm appearing on the DSC curves, the peak temperature (T_m) and the apparent enthalpy of fusion (ΔH_f) were determined. According to the enthalpy of fusion, the relative crystallinity of the crystallized membranes could be determined by:

$$X(\%) = \left(\frac{\Delta H}{\Delta H_{ref}}\right) \times 100\% \quad (1)$$

where ΔH_{ref} is the enthalpy of fusion of 100% crystallized PHBV polymer, it's assumed equal to $\Delta H_{ref} = 146 \cdot w_{PHB}$ J/g (w_{HB} is the weight fraction of 3HB in the copolymer). Here, the value of 146 J/g was from the enthalpy of fusion of 100% crystallized PHB polymer [27]. Because the core of the lamella of PHBV polymer with low 3HV content (<10 mol%) is composed of only the 3HB (3-hydroxybutyrate) units, the sequences of 3HV units are excluded from the lamella [28]. The enthalpy gain only upon the crystallization from the 3HB units is considered in this case.

2.4. Crystalline structure analysis

Small-angle X-ray scattering (SAXS) measurements were performed with an X-ray spectrometer (PSAXS-USH-WAXS-002, Osmic, USA) at room temperature to reveal the lamellar structure of the membranes. Thirty watts (30 W) of low power X-ray source/optic combination, provided Cu Kα radiation (the X-ray wavelength (λ) = 1.54 Å) with comparable intensity, was applied to form a focused beam from a rotating anode generator. X-ray source was operated at 45 kV and 0.67 mA. The X-ray beam spot size was $30 \times 30\ \mu m^2$. Specimens were cut into a $1.5 \times 1.5\ cm^2$ square and stacked to a requested thickness around 100 μm for the measurements. SAXS patterns were recorded in the range of $2\theta = 0$–3.5° with an increment of 0.0025°. The scattering profile was output as a plot of the scattering intensity (I) versus the scattering vector (q), $(4\pi/\lambda)\sin(\theta/2)$, where θ is the scattering angle and λ is the X-ray wavelength. The structures of semi-crystalline polymers are supposed to consist of periodically arranged crystalline lamellae. In the lamellar stack model, the long period represents the sum of the lamella thickness (L_c) and the amorphous layer thickness (L_a). The weight-average long period (L) can be calculated from the position of the peak maximum of the Lorentz-corrected profile [29] using Bragg's equation:

$$L = \frac{2\pi}{q_{max}} \quad (2)$$

2.5. Positron annihilation lifetime spectroscopy

Positron annihilation lifetime (PAL) experiments were carried out using an Ortec (Ametek, USA) fast–fast coincident timing spectrometer with temporal resolution of 300 ps (full width at half maximum of a single Gaussian), which was determined by measuring ^{60}Co (Isotope Products Laboratory, USA), and a channel width of 51 ps. Two identical specimens in the form of stacks of 500 μm thick with approximate area of $1.5 \times 1.5\ cm^2$ were sandwiched with a 20 μCi positron source (^{22}Na), which was prepared by evaporating $^{22}NaCl$ solution (Isotope Products Laboratory, USA) on a Kapton® (DuPont, USA) foil of 6 μm thickness. The sandwiched sample was enclosed into an aluminum heating block with a PID temperature controller (BTC-9100, Brainchild Electronic Co. LTD., Taiwan). Temperature dependence of PALS measurements was carried out during a thermal cycle in which the membrane was first heated from 25 to 35, 50, 70, and 90 °C, and then cooled down to 80, 60, 40, and 30 °C, respectively. The PAL spectrum measurement was performed after the temperature had been stabilized. In each spectrum a total of two million counts of positron annihilation were collected in about 2 h.

A PAL spectrum is composed of the lifetime of all positron and positronium components from birth to annihilation. In practice, the normalized lifetime spectrum is a convoluted differentiation of the normalized positron density $n(t)$. Thus, the lifetime τ_i and the intensity I_i values of the exponential components in the PAL spectrum can be extracted by deconvolution, background subtraction and then a non-linear fitting process. The spectrum which is composed of three lifetime components, τ_1, τ_2, τ_3, can be fitted by the equation:

$$N(t) = \sum \lambda_i I_i e^{-\lambda_i t} \quad (3)$$

where i (=1–3) is the number of each exponential term, I_i and λ_i ($= 1/\tau_1$) are the corresponding intensities (%) and annihilation rates (ns^{-1}), respectively. The PAL spectrum was analyzed into 3 discrete lifetimes using PATFIT computer programs [30]. It is plausible to assign τ_1 as the self-annihilation of p-Ps, τ_2 as the annihilation of free positrons and τ_3 as the annihilation of localized o-Ps with its surrounding electrons due to the pick-off annihilation. The annihilation rate of o-Ps is sensitive to the local environment, e.g., defects, voids, cracks in scale of nanometer. Particularly, o-Ps provides the major message on the free volume size, distribution, and quantity in a polymer and other matters. In addition, LT program [31] in the distribution mode assumed that the annihilation rate λ ($1/\tau$) follows a log-normal function was used to analyze an average o-Ps lifetime and also o-Ps lifetime dispersion (standard deviation, σ).

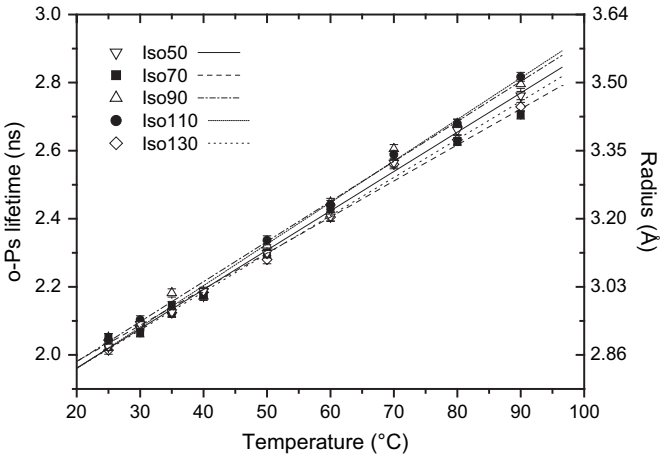

Fig. 1. Temperature dependence of the o-Ps lifetime of the PHBV membranes isothermally crystallized at various crystallization temperatures. On the right y-axis, the free volume radius is shown as converted from the o-Ps lifetime.

Table 1
The thermal expansion properties of the free volume parameters of the PHBV membranes isothermally crystallized at various T_cs.

Sample	α_{fv}[a] (10^{-2}/K)	$d\sigma/dT$[b] (10^{-3} ns/K)	$d(V_fI_3)/dT$ (10^{-2} Å^3/K)
Iso50	1.18 ± 0.03	6.1 ± 0.4	18.7 ± 0.7
Iso70	1.08 ± 0.03	6.0 ± 0.6	16.7 ± 0.4
Iso90	1.21 ± 0.04	6.1 ± 0.5	18.7 ± 0.6
Iso110	1.25 ± 0.03	5.4 ± 0.6	19.3 ± 0.3
Iso130	1.14 ± 0.03	5.0 ± 0.5	18.3 ± 0.3

[a] The values of the thermal expansion coefficient of the free volume are based on the mean volume of free volume holes (V_f) at 25 °C.
[b] σ is the standard deviation of the mean lifetime caused by the dispersion.

A relationship between the *o*-Ps lifetime and the free volume size is obtained from the overlap of the positron wave function in the open space and the electron wave function in the matrix [17]. If the free volume hole is simply regarded as a spherical well within an infinite potential and radius R_0 with an electron layer of thickness ΔR, a simple relationship between the lifetime (τ, in unit of ns) of *o*-Ps and the free volume radius (R) can be obtained [17,32]:

$$\tau_3 = \frac{1}{2}\left[1 - \frac{R}{R_0} + \frac{1}{2\pi}\sin\left(\frac{2\pi R}{R_0}\right)\right]^{-1} \quad (4)$$

where $R = R_0 - \Delta R$ in unit of Å. ΔR is a semi-empirical constant, and it is determined to be 1.66 Å for materials with well-defined size of cavity, such as zeolites and organic molecules [17].

The intensity of *o*-Ps lifetime (I_3) depends on the *o*-Ps formation probability which is related to the radiation chemistry while the *o*-Ps pick off takes place. If there is no significant variation of radiation chemistry in the polymer, the *o*-Ps intensity is related the amount of free-volume holes. Moreover, the relative fractional free volume (FFV) is expressed as follows:

$$\mathrm{FFV} = CV_fI_3 \quad (5)$$

where I_i (in %) is the *o*-Ps intensity. C is an empirical constant which was determined by calibrating with other physical parameters [33]. Herein, FFV from the PAL results should be considered as a relative value for the polymer of the same series since Eq. (5) was derived based on the Williams–Landel–Ferry (WLF) theory [33]. However, a precise determination of C is difficult to calibrate for semi-crystalline polymers due to the thermal history varies the degree of crystallinity [33]. Hence, the relative fractional free volume was estimated by the product of V_f and I_3 only, which is well accepted in literatures [34,35], for semi-crystalline PHBV polymer in this study.

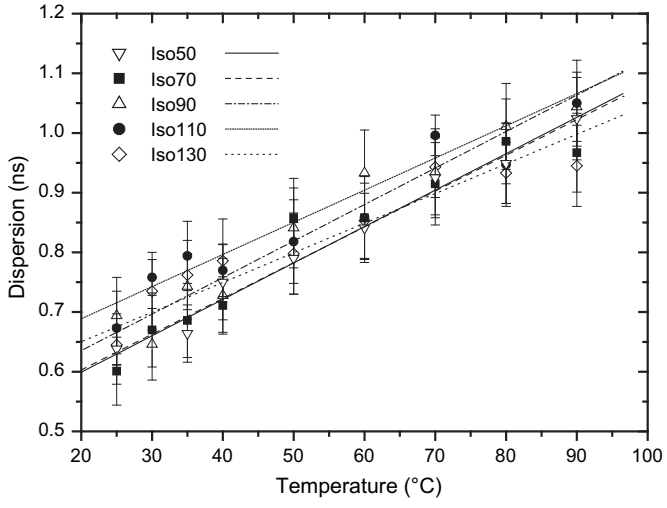

Fig. 2. Temperature dependence of the *o*-Ps lifetime dispersion of the PHBV membranes isothermally crystallized at various crystallization temperatures.

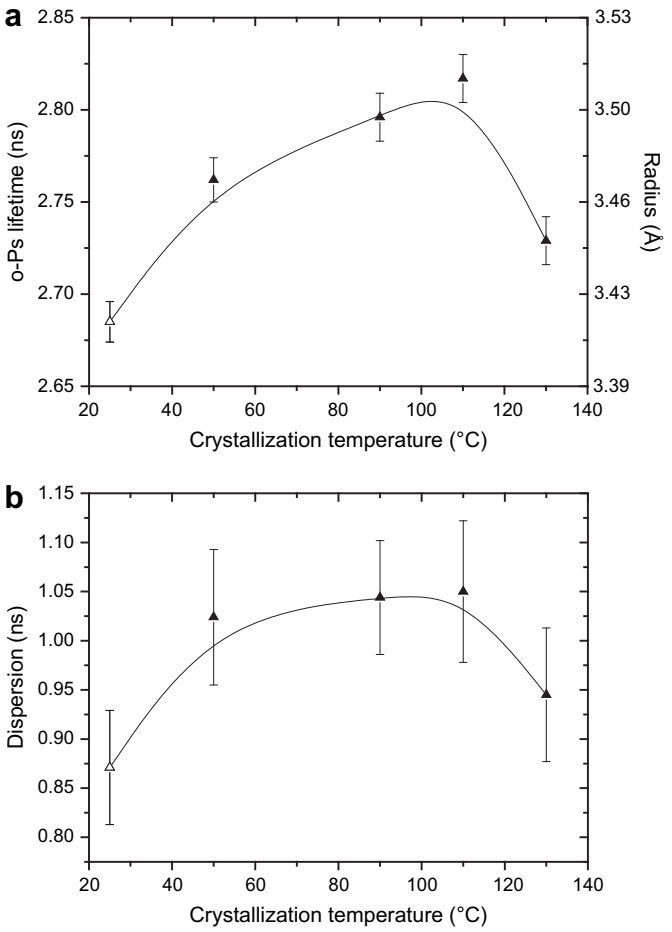

Fig. 3. Effect of crystallization temperatures on (a) the *o*-Ps lifetime and (b) the dispersion of the *o*-Ps lifetime of various PHBV membranes measured at 90 °C (closed symbol: isothermally crystallized membranes; open symbol: rapid-cooled membrane).

3. Results and discussion

Free volume properties of the PHBV membranes made via isothermal melt-crystallization process at various crystallization temperatures are discussed in this study. Over a temperature range of 25–90 °C, the *o*-Ps lifetime of each sample increases with temperature, and it follows the linear trend during a thermal cycle of heating and cooling runs as shown in Fig. 1. The radius of free volume hole could be calculated as appeared in the right *y*-axis of Fig. 1. From the results of PATFIT and LT programs, the change of the *o*-Ps lifetime values with temperature shows the same trend even though the values determined from LT were slight smaller than that from PATFIT. At higher temperatures, there is a significant difference between the size of the free volume of the membranes crystallized at various crystallization temperatures. Based on the following equation [36],

$$\alpha_{fv} = \left(\frac{1}{V_f}\right)\left(\frac{dV_f}{dT}\right) \quad (6)$$

the thermal expansion coefficient (α_{fv}) of the free volume above 25 °C in the rubbery region of the isothermally crystallized membranes is listed in Table 1. The thermal expansion coefficient

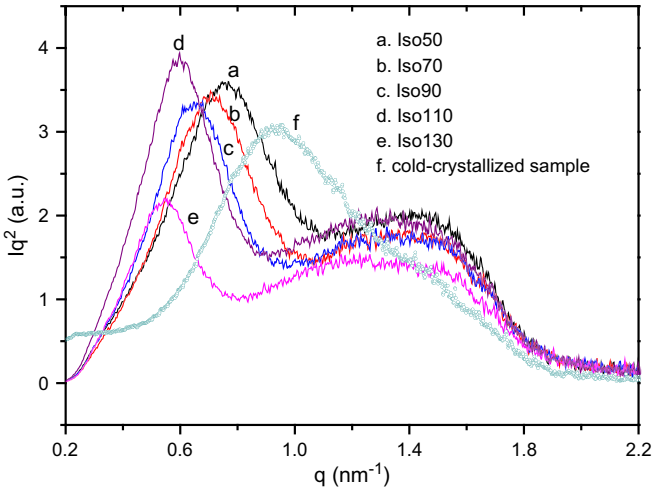

Fig. 4. Lorentz-corrected profile of various PHBV membranes.

was determined based on the mean volume of free volume holes (V_f) at 25 °C. It increased first and then decreased with the temperature at which the polymer was crystallized. In Fig. 2, the dispersion (σ) of *o*-Ps lifetime, which is the standard deviation of the *o*-Ps lifetime based on the log-normal distribution obtained from LT and means the size distribution of the free-volume hole, increases linearly with temperature during the thermal cycle. The slope of the *o*-Ps lifetime dispersion versus temperature ($d\sigma/dt$) is defined as the thermal expansivity of the free volume size distribution and listed in Table 1. Not following the results of the thermal expansion coefficient (α) of the free volume of various membranes, the values of $d\sigma/dt$ of all the membranes are close except the one of the membranes crystallized at 130 °C (Iso130 sample).

It's noticed that the variation of thermal expansion coefficients among the membranes shows a tendency similar to the dependence of crystallization rate on crystallization temperature (T_c) for PHBV polymer. Previous studies [21,28] showed that the growth rate of the crystalline spherulite of PHBV polymer with 6–8 mol% HV content had a maximum value at around 90 °C between 60 and 110 °C. It is speculated that a higher spherulite growth rate may induce greater thermal expansion of the free volume size of PHBV polymer. During the crystallization process, the segmental relaxation of the polymer is continuously reduced by crystal formation due to gradual transfer of a fraction of the amorphous material to the growing crystalline phase. When the primary crystallization is completed in a shorter time with a faster crystallization rate, which depends on the thermodynamic driving force and the molecular chain mobility at an appropriate T_c, the molecular chains in the amorphous region don't have enough time to pack densely. Therefore, higher thermal expansion coefficient of free volume and larger free volume size at higher temperature are obtained for the PHBV membranes isothermally crystallized at 90 and 110 °C than that crystallized at other T_cs as shown in Table 1 and Fig. 3(a), which is a plot of the *o*-Ps lifetime measured at 90 °C versus the

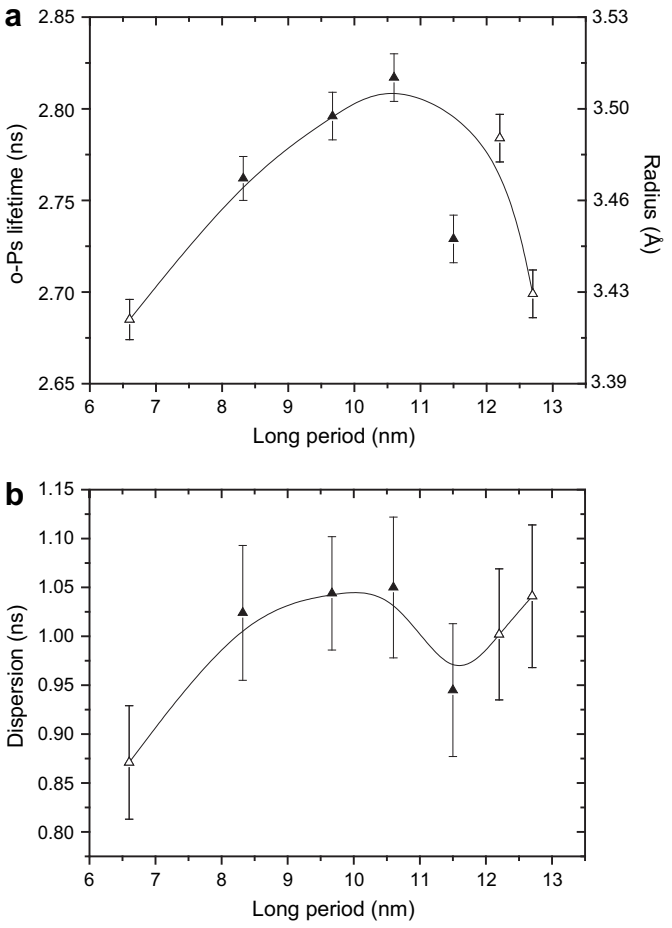

Fig. 5. Effect of long period on (a) the *o*-Ps lifetime and (b) the dispersion of the *o*-Ps lifetime of various PHBV membranes measured at 90 °C (closed symbol: isothermally crystallized membranes; open symbol: non-isothermally crystallized membranes).

crystallization temperature. Herein, only the results from the ones measured at 90 °C were discussed because the *o*-Ps lifetimes were not differentiable for various membranes at lower measuring temperatures. Besides, the *o*-Ps lifetime of a cold-crystallized membrane [26], which was crystallized at around room temperature (open symbol), is added into the figure as a reference. It was the smallest among all the membranes due to the relatively low crystallization rate.

The effect of crystallization temperature on the dispersion of *o*-Ps lifetime measured at 90 °C is shown in Fig. 3(b). We propose that the formation of bigger free volume during faster crystallization process is accompanied by broader free volume size distribution. Thus, the variation of *o*-Ps lifetime dispersion with crystallization temperature was found corresponding to that of the *o*-Ps lifetime. In addition, the values of the temperature dependence of the dispersion ($d\sigma/dt$) of all the isothermally crystallized

Table 2
Melting temperature, crystallinity, the scattering vector at which the maximum Lorentz-corrected intensity occurs, and the corresponding long period of various PHBV membranes.

Sample	T_m (°C)	X_c (%)	$q_{max,1}$ (nm^{-1})	$q_{max,2}$ (nm^{-1})	L_1 (nm)
Rapid-cooled	161 ± 2	56 ± 2	0.95 ± 0.01	–	6.6 ± 0.1
Iso50	162 ± 1	59 ± 2	0.76 ± 0.01	1.44 ± 0.01	8.32 ± 0.08
Iso70	164 ± 1	62 ± 2	0.71 ± 0.01	1.40 ± 0.01	8.91 ± 0.09
Iso90	165 ± 1	66 ± 1	0.65	1.32	9.67
Iso110	167 ± 0	68 ± 1	0.60 ± 0.01	1.28 ± 0.01	10.6 ± 0.1
Iso130	171 ± 1	71 ± 1	0.55 ± 0.01	1.22 ± 0.01	11.5 ± 0.1

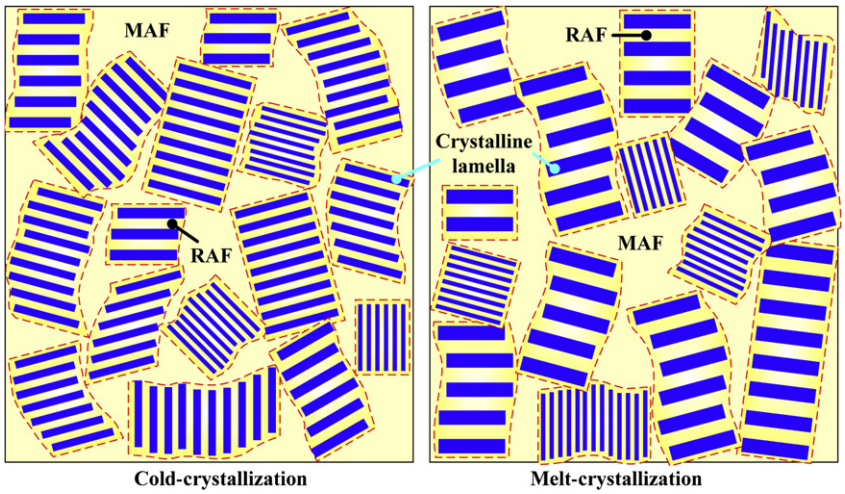

Scheme 1. The distribution of the RAF, MAF, and crystalline regions in the PHBV membranes with similar crystallinity via (a) cold- and (b) melt-crystallization procedures. (The yellow region is the amorphous phase; where the area enclosed within the dash lines is RAF and the area outside the dash lines is MAF. The solid blue lines are crystalline lamella). (For interpretation of the references to color in this scheme legend, the reader is referred to the web version of this article.)

membranes (Table 1) were very similar to that of the melt-crystallized membranes obtained from non-isothermal crystallization processes, i.e. 0.0060 ± 0.0005 ns/K [26]. In contrast, $d\sigma/dt$ of a cold-crystallized membrane was only 0.0039 ± 0.0004 ns/K. It can be concluded that the extent of the free volume size broadening in the measuring temperature range is affected by the crystallization procedure. Accordingly, it's necessary to consider the difference of the physical structure among the membranes crystallized through various procedures, such as lamellar periodicity.

Fig. 4 shows the profile of Lorentz-corrected intensity (Iq^2) probed by SAXS for various membranes. The Lorentz-corrected profile showed a broad peak at a higher q (the scattering vector, $(4\pi/\lambda)\sin(\theta/2)$) beside a distinct main peak at a lower q for all the isothermally crystallized membranes. This implied that there was a bimodal distribution of the thickness of the repeating lamellar/amorphous layers (long period) in these membranes. Herein, the distinct main peak at lower q of the Lorentz-corrected profile in the melt-crystallized membranes represented the crystalline morphology formed in the primary crystallization stage. The lamellar thickness and thickness of the lamellae/amorphous layers formed in this stage were thick and regular. During further isothermal crystallization process, small, thin and less regular lamellae were formed, which was detected from the broad peak at higher q in the Lorentz-corrected profile, due to the secondary crystallization. The main peak position (q_{max}) decreased with increasing of the crystallization temperature. It's noticed that the distribution of the main peak of Iso130 membrane was much narrower than that of all the others. Based on Bragg's law, the weight-average long period (L) was determined by Eq. (2). The values of q_{max} and L for various samples are listed in Table 2. The order of long period (from the main peak) was consistent with that of T_m for all the isothermally crystallized membranes (Table 2). Because thicker lamellae resulted in higher melting temperature [37,38], the membrane crystallized at higher temperature owned not only the thicker long period but also the thicker lamellar thickness. In addition, the melt-crystallized membranes underwent secondary crystallization at different crystallization temperatures during the later period of isothermal crystallization process. The lamellar periodicity formed in the secondary crystallization would follow the same trend in the primary crystallization. The broad peak

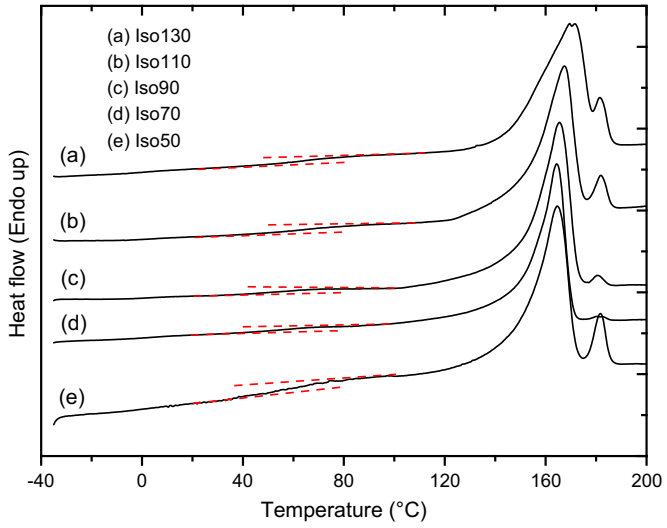

Fig. 6. DSC curves of the PHBV membranes isothermally crystallized at various crystallization temperatures.

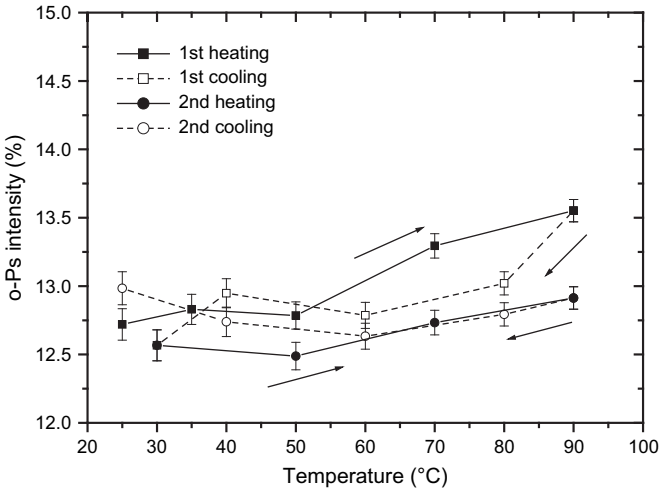

Fig. 7. Temperature dependence of the *o*-Ps intensity of the PHBV membranes isothermally crystallized at 90 °C during the thermal cycles (■: first run; ●: second run; closed symbol: heating step; open symbol: cooling step).

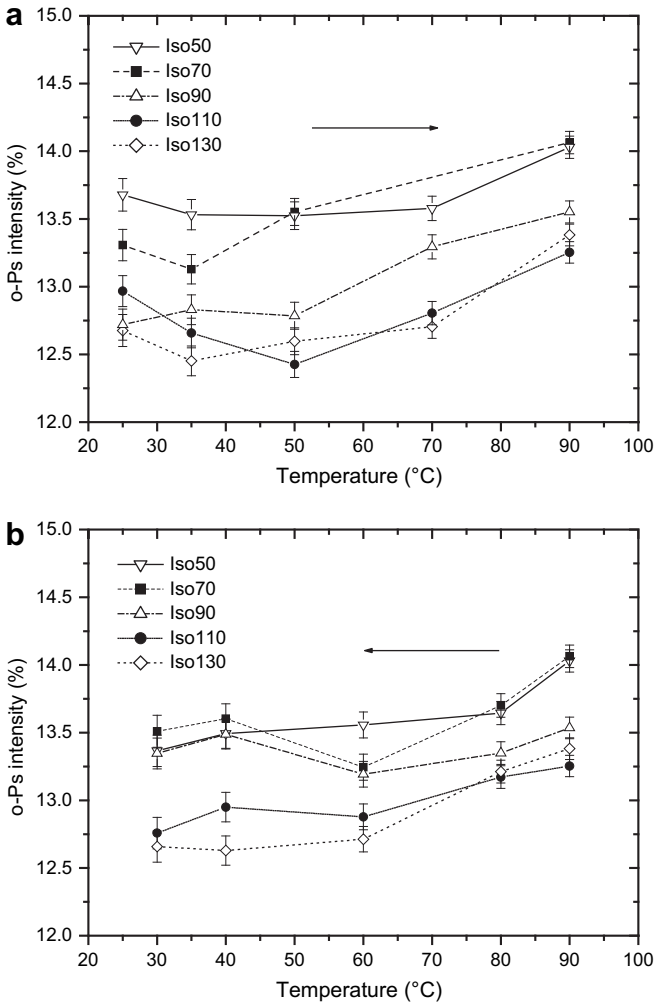

Fig. 8. Temperature dependence of the *o*-Ps intensity of the PHBV membranes isothermally crystallized at various crystallization temperatures: (a) heating run; (b) cooling run.

position at higher q decreased with increased crystallization temperature slightly, which decreased from 1.44 to 1.22 nm^{-1}, as shown in Table 2.

The effect of long period on the *o*-Ps lifetime and its dispersion are shown in Fig. 5. The results from non-isothermally crystallized membranes are added in order to discuss the relationship between lamellar structure and free volume size despite they were created by different crystallization processes. The long periods (from the main peaks) of the membranes crystallized via melt-crystallization with the slow-cooling and step-cooling processes are 12.7 and 12.2 nm, respectively [26]. The *o*-Ps lifetime measured at 90 °C did not have a proportional dependence on long period but showed a maximum value at an intermediate long period (Fig. 5(a)). This was because the free volume size depended on the crystallization temperatures as mentioned above. The dispersions of the *o*-Ps lifetime were distinguished into two groups, that of cold- and melt-crystallization membranes, respectively (Fig. 5(b)). Notably the dispersion of Iso130 membrane (the long period at 11.5 nm) was slightly smaller than other melt-crystallized membranes. It might be affected by the narrower distribution of the main Lorentz-corrected intensity peak (the long period) of Iso130 membrane than others (Fig. 4). Moreover, the smallest dispersion of the *o*-Ps lifetime among all the membranes was from the cold-crystallized membrane with a mono-distribution of long period and the thinnest average long period.

If lower crystallization temperature apparently results in thinner lamellae, it can be realized the number of lamellae in the lamellar stacks and the overall number of lamellar stacks in the cold-crystallized membrane are larger than that in the melt-crystallized membranes with similar level of crystallinity. This leads to much larger amount of amorphous phase constrained between the crystalline lamellae in the case of cold-crystallized membranes [13,34]. As shown in Scheme 1, which is the situation of three-phase (MAF, RAF, and crystalline phases) model in the membranes prepared via cold- and melt-crystallization procedures, the cold-crystallized membrane is proposed that it has a larger amount of interlamellar amorphous phase (RAF) and smaller domain size of the interstack amorphous phase (MAF) than that of the melt-crystallized membrane with a specific crystallinity. Therefore, the free volume size of cold-crystallized membrane is limited and hard to expand upon heating, which represents by the smaller thermal expansivity of free volume size and size distribution of cold-crystallized membrane, due to the constraint of the lamellar morphology. In addition, the melt-crystallized membranes owned bimodal distribution of the repeating lamellar/amorphous layers and created various size of spaces in the interlamellar or interstack regions. The difference of the crystalline morphology resulted in various size of free volume located in the RAF and MAF in the membranes prepared from various crystallization procedures. Therefore, the free volume size distribution of the melt-crystallized membranes is broader than that of cold-crystallized ones. Summarily, the cold- and melt-crystallization procedures resulted in two kinds of distributions of long period and a difference of the amount of RAF so that the *o*-Ps lifetime dispersion or the free volume size distribution could be distinguished into two groups.

Herein, a significant RAF can be observed from the heat capacity jump according to the DSC trace (Fig. 6), and the corresponding $\Delta C_{p,RAF}$ is about 0.2 J/g °C. A previous study [13] addressed the estimation of the weight portion of the RAF for poly(ethylene terephthalate) (PET) by a DSC experiment. The weight portion of the RAF is determined by providing information of the heat capacity jump of fully amorphous PET polymer, the heat capacity jump of the semi-crystalline PET at T_g, and the weight fraction of crystalline phase. In this study, however, the weight portion of the RAF of the semi-crystalline PHBV polymer is unavailable from this method. The heat capacity jump of fully amorphous PHBV polymer

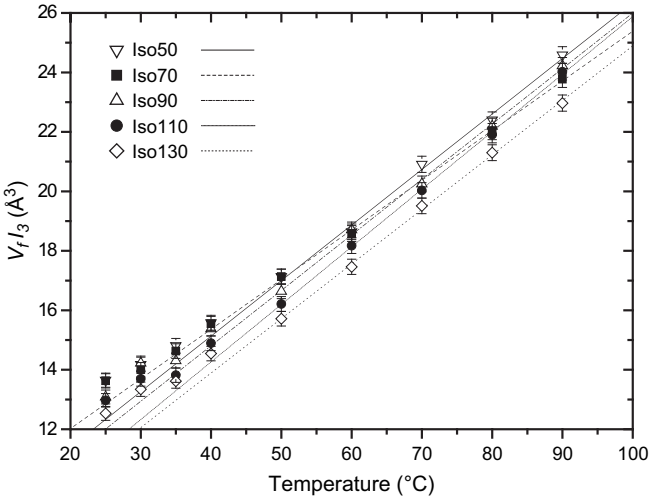

Fig. 9. Temperature dependence of the relative FFV ($V_f I_3$) of the PHBV membranes isothermally crystallized at various crystallization temperatures.

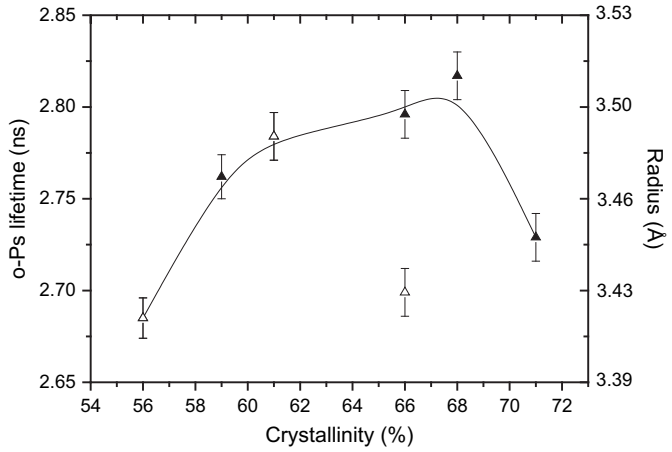

Fig. 10. Effect of crystallinity on the *o*-Ps lifetime of PHBV membranes measured at 90 °C (closed symbol: isothermally crystallized membranes; open symbol: non-isothermally crystallized membranes).

is hard to obtain due to the low T_g and fast crystallization rate of this polymer. It may be possible to use the heat capacity jump at T_g of PHBV polymer with known crystallinity to deduce the heat capacity jump of a fully amorphous sample. Even though, the T_g corresponded to MAF may not be clear in the case of high crystallinity sample. The accurate determination of the RAF and MAF portion of PHBV polymer is very difficult if it's still possible.

The variations of the *o*-Ps intensity of the membranes isothermally crystallized at various T_cs during the cycles of heating and cooling processes were discussed. *o*-Ps intensity increased slightly with temperature above 70 °C and then decreased slightly during the cooling run, nevertheless, the amount of free volume would not increase significantly during the thermal process in the measuring temperature range (Fig. 7). In previous studies, the number density of holes determined due to combination of Simha–Somcynsky theory with PALS has been addressed that does not depend on temperature [10,39]. As presented in our previous study [40], the I_3 of the PHBV membrane which was isothermal crystallized at 90 °C showed a relatively constant value in the range from room temperature to around 70 °C. The immobilization of amorphous polymer chains around the less perfect crystals results in the vitrification of the RAF during crystallization. With a further increase of temperature, the mobility of segment at fold surface of the crystallites would increase observably. It led to the rearrangement of molecular chain packing above this temperature so that new free volume holes were created, the *o*-Ps intensity increased from 13.88 to 16.25% when the measuring temperature increased from 90 °C to 190 °C. In this study, according to the results of DSC trace, a transition state of the RAF was observed due to the devitrification of the RAF between 40 and 80 °C as shown in Fig. 6. Therefore, *o*-Ps intensity showed a relatively constant value in the range from room temperature to around 70 °C and then increased due to the change of physical structure. A reversible behavior of the *o*-Ps intensity in two runs of the thermal cycles, which included first heating, first cooling, second heating, and second cooling, was observed as shown in Fig. 7. During the second cycle, the thermal cycles might create an annealing effect in the membrane, the crystallinity increased slightly, so that the *o*-Ps intensity didn't increase with temperature and kept relatively close to a constant in the range of 25–90 °C. In addition, the *o*-Ps intensity decreased with increasing crystallization temperature during both the heating and the cooling runs (Fig. 8) due to the change of crystallinity (Table 2). The relationship between the positron annihilation parameters and the crystallinity will be discussed later. Furthermore, a linear correlation between the relative FFV (V_fI_3) and temperature was established above 50 °C (Fig. 9). As the trends of *o*-Ps intensity, the relative FFV decreased with increasing crystallization temperature. Although there are other arguments against relating I_3 with FFV since I_3 is affected by radiation chemistry of polymer systems [39,41], the I_3 value of PHBV polymer should still be included into the calculation of FFV to explain the effect of crystallization temperature and/or crystallinity on the FFV of PHBV membranes. Otherwise, the data of PHBV membranes could not be explained well if one ignores the I_3 part in calculating FFV. Therefore, a product of V_f and I_3 is used to show the relative FFV of PHBV membranes in this study. Furthermore, not following the trend of the thermal expansion coefficients of the free volume size (α_{fv}), the thermal expansivities of the FFV ($d(V_fI_3)/dT$) were not significantly varied between the membranes isothermally crystallized at various T_cs (Table 1). It's noticed the relative FFV measured at lower temperatures are deviated from extrapolated ones from the linear correlations of the relative FFV data versus temperature for all the membranes. We speculate that this region is close to the T_g ($\sim$0 °C) of PHBV so that the molecular motion may be rather slow in the transition phase. The thermal expansivity was lower than that at a higher temperature range, but still higher than that in the glassy state. These behaviors have been observed in the literature [42,43].

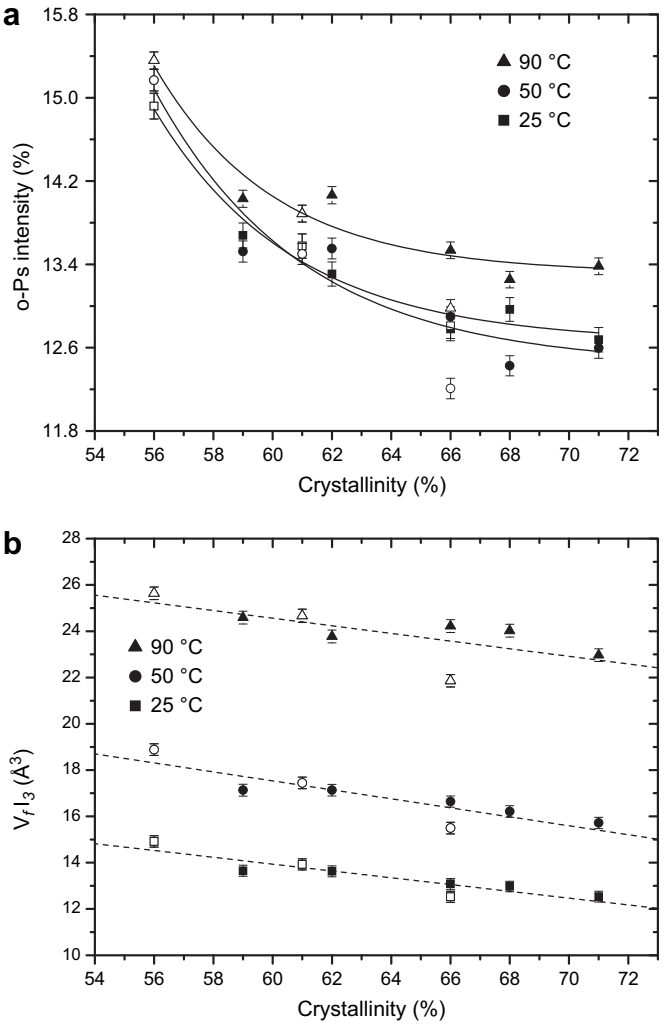

Fig. 11. Effect of crystallinity on (a) the *o*-Ps intensity and (b) the relative FFV (V_fI_3) of various PHBV membranes measured at 25, 50, and 90 °C (closed symbol: isothermally crystallized membranes; open symbol: non-isothermally crystallized membranes).

The effects of crystallinity on the free volume properties were established as shown in Figs. 10 and 11. In the range between 56% and 71% of the crystallinity (X_c), *o*-Ps lifetime did not vary significantly at lower measuring temperatures. This behavior has been reported in the studies of other semi-crystalline polymers [44,45]. However, the difference of the *o*-Ps lifetime measured at 90 °C among the membranes with different crystallinity was observed (Fig. 10) due to the difference of thermal expansion behaviors as presented above. There was a notable difference between the *o*-Ps lifetimes of Iso90 sample and the slow-cooled membrane although both had the same crystallinity (66%). Because the free volume size of membrane was controlled by the crystallization rate, the smaller free volume size (or *o*-Ps lifetime) of the slow-cooled membrane was caused by the slow-cooling process with slower crystallization rate than that of the membrane crystallized at 90 °C. Moreover, the *o*-Ps intensity and the relative FFV showed as a function of crystallinity at all measuring temperatures as shown in Fig. 11. As a consequence of a decreased crystallinity, the amount of amorphous region raised more free volume holes, and led to higher relative FFV of a polymer. This phenomenon has been widely discussed in the literature [16,24]. Consequently, the size of the free volume was decided during the crystallization process, which was a kinetic controlled behavior. The total amount of free volume and fractional free volume was controlled by the final crystallinity of the membranes.

4. Conclusions

In this study, the relationship between free volume properties and structure of the PHBV membranes prepared via various crystallization conditions was studied. The formulation of a three-phase model, which included crystalline, RAF, and MAF phases, was applied to interpret the free volume characteristics of PHBV membranes which were obtained from PAL spectroscopy. Observations of the crystalline structure and crystallinity of the membranes controlled by the cold- and melt-crystallization processes provided the basis of a structural interpretation for this model.

The temperature dependence of the free volume size, size distribution, amount of the free volume, and fractional free volume which presented by the *o*-Ps annihilation parameters of the isothermally crystallized PHBV membranes over a temperature range of 25–90 °C were discussed. A strong dependence of the thermal expansion coefficients of the free volume of the isothermally crystallized membranes on the crystallization temperatures was found. Faster crystallization rate, which depended on the crystallization temperature, would result in looser molecular chain packing in the amorphous region due to shorter crystallization time. Therefore, the molecular chains easily move and rearrange at higher temperatures; higher thermal expansion coefficient and larger size of the free volume at higher measuring temperature were observed. A bimodal distribution of the lamellar periodicity and thicker lamellar thickness, which affected the amount of RAF, were detected for melt-crystallized membranes led to much broad distribution of the free volume and larger thermal expansivity of free volume size distribution than that of cold-crystallized ones.

The relatively constant and reversible value of the *o*-Ps intensity during the heating and cooling processes in the measuring temperature range could be understood assuming that the number of free volume holes in the same structure would not change with temperature. The existence of the RAF was demonstrated by DSC trace as the transition state of the RAF between 40 and 80 °C. After the devitrification of the RAF, *o*-Ps intensity increased above 70 °C due to the change of physical structure. The *o*-Ps intensity and the relative FFV decreased with increasing of crystallization temperature. It could be correlated to the final crystallinity reached during crystallization. This was obviously associated with a dense molecular packing in crystals which prohibited the formation of free volume inside. Therefore, good correlations between relative FFV and crystallinity were established at various measuring temperatures. In conclusion, a model of the free volume formation during the crystallization process was developed. Free volume size and thermal expansion behavior of the free volume in PHBV membranes were influenced by the kinetics of crystallization. The size distribution of free volume was associated with the crystalline structures which were dominated by the crystallization conditions. Generally, the final crystallinity determined the total amount of free volume and fractional free volume, but didn't show a direct effect on the size or size distribution of free volume.

Acknowledgments

This work was supported by the National Science Council of the Republic of China through the grants of NSC96-2221-E-155-074. The authors thank Prof. Y.C. Jean and Dr. Hongmin Chen of the University of Missouri-Kansas City for their kind assistances on many PAL spectroscopy techniques.

References

[1] Ferry JD. Viscoelastic properties of polymer. 3rd ed. New York: Wiley; 1980.
[2] Doolittle AK, Doolittle DB. J Appl Phys 1957;28:901–9.
[3] Kovacs A. Adv Polym Sci 1964;3:394–507.
[4] Hutchinson JM. In: Haward RN, Young RJ, editors. The physics of glassy polymer. London: Chapman & Hall; 1997. p. 85.
[5] Bauwens JC. In: Brostow W, Corneliussen RD, editors. Failure of plastics. New York: Hanser; 1986.
[6] Crank J, Park GS. Diffusion in polymers. London: Academic Press; 1968.
[7] Khoury F, Passaglia E. The morphology of crystalline synthetic polymers. In: Hannay NB, editor. Treatise on solid state chemistry, vol. 3. New York: Plenum Press; 1976. p. 335.
[8] Suzuki H, Grebovicz J, Wunderlich B. Br Polym J 1985;17:1–3.
[9] Šics I, Ezquerra TA, Nogales A, Baltá-Calleja FJ, Kalniņš M, Tupureina V. Biomacromolecules 2001;2:581–7.
[10] Dlubek G, Gupta AS, Pionteck J, Häßler R, Krause-Rehberg R, Kaspar H, et al. Polymer 2005;46:6075–89.
[11] Hu YS, Liu RYF, Zhang LQ, Rogunova M, Schiraldi DA, Nazarenko S, et al. Macromolecules 2002;35:7326–37.
[12] Kilburn D, Bamford D, Lüpke T, Dlubek G, Menke TJ, Alam MA. Polymer 2002;43:6973–83.
[13] Lin J, Shenogin S, Nazarenko S. Polymer 2002;43:4733–43.
[14] Gedde UW. Polymer physics. London: Chapman & Hall; 1995.
[15] Chen H, Cheng ML, Jean YC, Lee LJ, Yang J. J Polym Sci B Polym Phys 2008;46:388–405.
[16] Mallon PE. Application to polymers. In: Jean YC, Mallon PE, Schrader DM, editors. Principles and application of positron and positron chemistry. Singapore: World Scientific; 2003. p. 253.
[17] Nakanishi H, Wang SJ, Jean YC. In: Sharma SC, editor. Positron annihilation studies of fluids. Singapore: World Scientific; 1988. p. 292.
[18] Yampolskii Y, Shantarovich V. Positron annihilation lifetime spectroscopy and other methods for free volume evaluation in polymers. In: Yampolskii Y, Pinnau I, Freeman BD, editors. Materials science of membranes for gas and vapor separation. New York: Wiley Interscience; 2006. p. 191.
[19] Mogensen OE. Positron annihilation in chemistry. Berlin: Springer-Verlag; 1995.
[20] Verhoogt H, Ramsay BA, Favis BD. Polymer 1994;35:5155–69.
[21] Scandola M, Ceccorulli G, Pizzoli M, Gazzano M. Macromolecules 1992;25:1405–10.
[22] Miguel O, Barbari TA, Iruin JJ. J Appl Polym Sci 1999;71:2391–9.
[23] Miguel O, Iruin JJ. J Appl Polym Sci 1999;73:455–68.
[24] Dlubek G, Stejny J, Lüpke TH, Bamford DKP, Hübner CH, Alam MA, et al. J Polym Sci B Polym Phys 2002;40:65–81.
[25] Machado J, Silva GG, De Oliveira FC, Lavail RL, Rieumont J, Licinio P, et al. J Polym Sci B Polym Phys 2007;45:2400–9.
[26] Cheng ML, Sun YM. J Polym Sci B Polym Phys 2009;47:855–65.
[27] Barham PJ, Keller A, Otun EL, Holmes PA. J Mater Sci 1984;19:2781–94.
[28] Yoshie N, Saito M, Inoue Y. Macromolecules 2001;34:8953–60.
[29] Kavesh S, Schultz JM. J Polym Sci A Polym Chem 1970;8:243–76.
[30] PATFIT package. Denmark: Riso National Laboratory; 1989.
[31] Kansy J. Nucl Instrum Methods Phys Res A 1996;374:235–44.
[32] Tao SJ. J Chem Phys 1972;56:5499–510.
[33] Jean YC. Microchem J 1990;42:72–102.

[34] Olson BG, Lin J, Nazarenko S, Jamieson AM. Macromolecules 2003;36:7618–23.
[35] Sun N, Liu J, Dull T, Yee AF. J Polym Sci B Polym Phys 2007;45:1410–7.
[36] Okamoto K, Tanaka K, Katsube M, Kita H, Ito Y. Bull Chem Soc Jpn 1993;66:61–8.
[37] Cser F. J Appl Polym Sci 2001;80:358–66.
[38] Dlugosz J, Fraser GV, Grubb D, Keller A, Odell JA, Goggin L. Polymer 1976;B17:471–80.
[39] Dlubek G, Bondarenko V, Al-Qaradawi IY, Kilburn D, Krause-Rehberg R. Macromol Chem Phys 2004;205:512–22.
[40] Cheng M-L, Sun Y-M, Chen H, Jean YC. Polymer 2009;50:1957–64.
[41] Maurer FHJ, Schmidt M. Radiat Phys Chem 2000;58:509–12.
[42] Abdel-Hady EE, Mohamed HFM, Fareed SS. Phys Stat Solidi (c) 2007;4:3907–11.
[43] Wilkinson NJ, Archer D, Clayton JM, Usmar SG, Alam MA. Mater Sci Forum 1992;105–110:1819–22.
[44] Lind JH, Jones PL, Pearsall GW. J Polym Sci A Polym Chem 1986;24:3033–47.
[45] Nakanishi H, Jean YC, Smith EG, Sandreczki TC. J Polym Sci B Polym Phys 1989;27:1419–24.